

**Chimera states in networks of type-I Morris-Lecar neurons**Ali Calim,<sup>1,\*</sup> Philipp Hövel,<sup>2,3</sup> Mahmut Ozer,<sup>4</sup> and Muhammet Uzuntarla<sup>1,†</sup><sup>1</sup>*Department of Biomedical Engineering, Bulent Ecevit University, Zonguldak, Turkey*<sup>2</sup>*School of Mathematical Science, University College Cork, Cork T12 XF64, Ireland*<sup>3</sup>*Institut für Theoretische Physik, Technische Universität Berlin, Hardenbergstraße 36, 10623 Berlin, Germany*<sup>4</sup>*Department of Electrical and Electronics Engineering, Bulent Ecevit University, Zonguldak, Turkey*

(Received 3 September 2018; revised manuscript received 8 November 2018; published 21 December 2018)

Chimeras are complex spatiotemporal patterns that emerge as coexistence of both coherent and incoherent groups of coupled dynamical systems. Here, we investigate the emergence of chimera states in nonlocal networks of type-I Morris-Lecar neurons coupled via chemical synapses. This constitutes a more realistic neuronal modeling framework than previous studies of chimera states, since the Morris-Lecar model provides biophysically more relevant control parameters to describe the activity in actual neural systems. We explore systematically the transitions of dynamic behavior and find that different types of synchrony appear depending on the excitability level and nonlocal network features. Furthermore, we map the transitions between incoherent states, traveling waves, chimeras, coherent states, and global amplitude death in the parameter space of interest. This work contributes to a better understanding of biological conditions giving rise to the emergence of chimera states in neural medium.

DOI: [10.1103/PhysRevE.98.062217](https://doi.org/10.1103/PhysRevE.98.062217)**I. INTRODUCTION**

Synchronization is widely assumed to be essential for the proper functioning of a large variety of natural and artificial systems, ranging from physical experiments to chemical reactions and physiological processes. Prime examples include coupled lasers [1], Josephson junctions [2], oxidation and catalytic surface reactions [3,4], genetic oscillator networks [5], and neural systems [6]. For decades, synchronization in neural systems has remained a very popular topic of research, because it is considered as a brain mechanism underlying many behavioral and cognitive functions, e.g., attention selection, information processing, and neural control of movement [7–11]. Furthermore, neural synchronization is proposed to be responsible for formation and dissolution of functional brain networks performing multiple vital tasks, such as visual perception, sleeping, and memory in the brain [12–14]. Considering its relative consequences, it is critical to understand how neural synchronization is organized or conserved and how it affects the neural information coding or propagation.

However, synchronized population activity is not perpetually desirable and pervasive in every region of the brain [15,16]. For instance, the cortex operates in a highly asynchronous state during waking and REM sleep, in which low-frequency oscillations, i.e., delta activity, are adequately inhibited [17]. The subthalamic nucleus, a specific location in the basal ganglia, is another example of this observation. It exhibits desynchronized electrical activity in the beta frequency band as an indicator of movement preparation [18].

In some cases, these two common states, namely, synchronization and desynchronization, could be present within the same neuronal circuitry at the same time [19,20]. Several recent experimental and clinical studies confirm that such a coexistence occurs in the brain, more specifically during unihemispheric sleep [21,22], epileptic seizures [23,24], and bump states [25,26] observed in *in vitro* preparations. The idea first surfaced in the pioneering work of Kuramoto, in which this surprising collective behavior was studied in identical phase oscillators with nonlocal interactions [27]. Following the first report of such an intriguing hybrid behavior, Abrams and Strogatz named this emergent dynamical phenomenon *chimera state* [28]. In chimeras, coupled dynamical elements exhibit extraordinary spatiotemporal patterns splitting the system into two subpopulations: one synchronized and phase locked, the other desynchronized and incoherent. This symmetry-breaking behavior has been studied in a variety of complex dynamical systems and has attracted growing attention in neural system studies from both theoretical and experimental perspectives [28–31]. Aside from its experimental evidences in optical [32], chemical [33], mechanical [34,35], electronic [36,37], electrochemical oscillator systems [38–40], extensive theoretical and numerical studies exploring chimera states have only recently been carried out in the field of neuroscience [41–48].

Hizanidis *et al.* investigated chimera states in modular neural networks based on the connectome of *Caenorhabditis elegans* [49]. They showed that chimeralike states spontaneously emerge with a suitable tuning of electrical and chemical coupling strengths. Moreover, it was also reported that an important system component, which leads to emergence of chimeras, is the largest community in constructed modular networks. In another work, Majhi *et al.* analyzed chimera states in a two-layer neural network, considering

\*ali.calim@hotmail.com

†muzuntarla@yahoo.com

Hindmarsh-Rose neurons coupled via electrical and chemical synapses [50]. They showed that the emergence of chimera states depends significantly on chemical synapses, not electrical ones. They also emphasized the importance of chemical synaptic transmission delays and illustrated that chimera states appear in a larger region in a two-dimensional parameter space (coupling range versus chemical synaptic strength) due to the increasing values of delay in the synaptic transmission between the layers. Omelchenko *et al.* studied robustness of chimera state adding heterogeneity into single neuron dynamics and network topology [51]. They demonstrated that chimera state maintains in the system of inhomogeneous FitzHugh-Nagumo neurons with nonlocal coupling topology by introducing small diversities into intrinsic cellular properties. They also showed that random structural irregularities of the network topology do not destroy the chimera state up to a certain limitation of random links.

It is well known from experimental and theoretical studies that one of the most important intrinsic features of neural dynamics is excitability [52–55]. It plays a basic but important role in achieving biological functions of the nervous system by determining firing and resting behaviors. In fact, the excitability is determined by a bifurcation parameter that changes the dynamic behavior of a neuron from a quiescence state to a regularly spiking regime. In this sense, neurons are mainly classified into two types according to frequency response characteristics to a constant bias current: type-I excitability with a continuous frequency versus bias current curve related to a saddle-node infinite-period bifurcation of equilibria and type-II excitability with a discontinuous frequency versus bias current curve connected to a Hopf bifurcation. At the bifurcation point, neurons of type-I excitability begin to exhibit self-sustained oscillation with an almost zero frequency. In contrast, type-II neurons switch from quiescence state to repetitive firing with a finite frequency. Apart from the firing frequency as a response to an external bias current, type-I and type-II neurons differ in several ways, such as their phase response curves to excitatory impulsive perturbations, their frequency response properties to periodic stimulus, i.e., integrator or resonator behavior, or their coefficients of variation of interspike intervals to stochastic inputs [56].

The vast majority of chimera studies in the neuroscience literature to date have focused on the emergence of this state in neural systems of type-II excitability. Chimera state has been detected and deeply analyzed in populations of FitzHugh-Nagumo [57] and Hindmarsh-Rose [58] neurons, which are prominent models for this class of neural excitability. However, chimera research on neural systems with type-I excitability has been considered only with a generic neuron model, the saddle-node infinite period oscillator [59]. To ensure biophysical relevance and achieve realistic modeling, taking into account ion current dynamics is crucial for neural systems which would potentially evolve into chimera state since above-mentioned phenomenological neuron models do not involve ion currents and gating features.

In this paper, we address this issue and report for the first time the emergence of chimera state in a nonlocally coupled neural population of Morris-Lecar model exhibiting type-I excitability but not bistability. As for the synaptic communication within the network, excitatory chemical coupling scheme

is considered. Using this modeling framework, we show the existence of peculiar chimera state as well as other emergent system regimes (incoherent state, traveling wave, coherent state and global amplitude death) by exclusively scanning the excitability level of individual units and the interaction intensity in nonlocal network associated with coupling range and synaptic strength.

The rest of the paper is organized as follows: In the next section, we introduce the model, that is, a set of  $N$  nonlocally coupled Morris-Lecar neurons, and the methods used for the characterization of chimera states in terms of firing frequency and strength of incoherence. Section III includes the main results and frames the conditions for the appearance of chimera states. In Sec. III A, we present a bifurcation analysis of the Morris-Lecar model. In Sec. III B, variation of dynamical behaviors was analyzed depending on the level of excitability. In Sec. III C, the influences of nonlocal network features on the appearance of chimera states were investigated and explained by producing detailed parameter maps that reveal the behavioral transitions between different network states. Furthermore, we went into a minute examination of chimeric behavior to identify its key characteristics. Finally, the main conclusions are summarized in Sec. IV.

## II. MODELS AND METHODS

We consider a nonlocal network of Morris-Lecar neurons coupled with excitatory chemical synapses. The membrane potential of a neuron in the network is modeled based on the two-variable Morris-Lecar equations as follows [60–63]:

$$C \frac{dV_i}{dt} = g_{Ca} m_i^\infty (E_{Ca} - V_i) + g_K w_i (E_K - V_i) + g_L (E_L - V_i) + I_0 + I_i^{\text{syn}}, \quad (1)$$

$$\frac{dw_i}{dt} = \phi(w_i^\infty - w_i) \cosh\left(\frac{V_i - \beta_w}{2\gamma_w}\right), \quad (2)$$

$$m_i^\infty(V_i) = 0.5 \left[ 1 + \tanh\left(\frac{V_i - \beta_m}{\gamma_m}\right) \right], \quad (3)$$

$$w_i^\infty(V_i) = 0.5 \left[ 1 + \tanh\left(\frac{V_i - \beta_w}{\gamma_w}\right) \right], \quad (4)$$

where  $i = 1, 2, \dots, N$  is the neuron index.  $V_i$  denotes the membrane potential, and  $I_0$  is the externally applied bias current.  $w_i$  and  $m_i$  are the fraction of open  $K^+$  and  $Ca^{+2}$  channels, respectively.  $C$ ,  $\phi$ ,  $\beta_m$ ,  $\gamma_m$ ,  $\beta_w$  and  $\gamma_w$  are constants.  $g_{Ca}$ ,  $g_K$  and  $g_L$  represent conductances for calcium, potassium and leak channels, respectively.  $E_{Ca}$ ,  $E_K$  and  $E_L$  denote the corresponding equilibrium potentials (see Table I). Last,  $I_i^{\text{syn}}$  denotes the total synaptic current received by neuron  $i$  from its nonlocal interactions.

TABLE I. Morris-Lecar model parameters for type-I excitability.

$g_{Ca} = 1 \text{ mS/cm}^2$	$g_K = 2 \text{ mS/cm}^2$	$g_L = 0.5 \text{ mS/cm}^2$
$E_{Ca} = 100 \text{ mV}$	$E_K = -70 \text{ mV}$	$E_L = -50 \text{ mV}$
$\beta_m = -1 \text{ mV}$	$\beta_w = 10 \text{ mV}$	$C = 1 \text{ } \mu\text{F/cm}^2$
$\gamma_m = 15 \text{ mV}$	$\gamma_w = 14.5 \text{ mV}$	$\phi = 1/3$

Transmission of an electrical stimulus from a presynaptic neuron to a postsynaptic cell takes place in either electrical or chemical synapses. Based on their electrophysiology, these can be defined as linear and nonlinear coupling, respectively. In an electrical synapse, ions flow directly from one cell into another and the synaptic activity is bidirectional. In a chemical synapse, however, the signal transmission occurs in one direction with complex mechanisms where molecules of released excitatory or inhibitory neurotransmitters from presynaptic neuron diffuse across the synaptic cleft and bind to receptor proteins on the postsynaptic terminal. Since excitatory synapses, compared to inhibitory and electrical ones, constitute the vast majority of the communication pathways in nervous system [64], we consider excitatory coupling as the basis of the interaction dynamics in our system setup. The total excitatory synaptic current is calculated by summing over nonlinear inputs arriving from all neighboring neurons based on the following equation:

$$I_i^{\text{syn}} = g \sum_{j=i-R}^{i+R} x_j, \quad (5)$$

where  $g$  is the synaptic strength. The summation index is to be taken modulo  $N$ .  $R$  denotes the number of nearest neighbors of each neuron  $i$  in two direction, with the limiting cases of  $R = 1$  and  $R = N/2$  corresponding to ring and global network topologies, respectively. Any value of  $R$  in between these two limits is regarded as nonlocal coupling. We conveniently scale this parameter to control the size of nonlocal system division, which defines a nonlocal coupling radius  $r = R/N \in (1/N, 0.5)$ . The quantity  $x_j$  is the fraction of effective neurotransmitter resources released by presynaptic terminal into the synaptic cleft in the active state of the synapse, and it obeys the following equation:

$$\frac{dx_j}{dt} = -\frac{x_j}{\tau} + u_j \delta(t - t_j), \quad (6)$$

where  $\tau$  is the time constant representing the decay of active resources in presynaptic terminals.  $u_j$  denotes the fraction of releasable vesicles, that belong to the readily releasable pool, activated upon an action potential arrival. We set these parameters as  $\tau = 6$  ms and  $u_j = 0.2$ . Finally,  $t_j$  is the firing time of presynaptic  $j$ th neuron defined by the upward crossing of the membrane potential past a threshold of 10 mV.

To study the existence of a chimera state, we employ a widely used indicator to quantify its properties: the average firing frequency computed by  $f_i = F_i/\Delta T$ . Here,  $F_i$  is the number of firings of the  $i$ th neuron within a period of time  $\Delta T$  after a sufficient transient. Furthermore, we also employ an additional quantitative measure called strength of incoherence ( $S$ ) recently proposed by Gopal *et al.* [65], which allows us to statistically identify different dynamical states in the population as a function of a system parameter of interest [66–70]. To obtain the  $S$  measure, we first compute the local fluctuation of membrane potentials:  $z_i = V_i - V_{i+1}$  with the index be taken modulo  $N$ . Next, we divide all neurons in the network into  $M$  groups of equal length  $n = N/M$ . We choose  $M = 50$  for a ring network of 1000 elements, which we find to be optimal. Then, to quantify self-correlation of each group, the time-averaged local standard deviation of  $z_i$  is calculated

by the following equation:

$$\sigma(m) = \left\langle \sqrt{\frac{1}{n} \sum_{k=n(m-1)+1}^{nm} [z_k - \langle z \rangle]^2} \right\rangle, \quad (7)$$

where  $m = 1, 2, \dots, M$  and  $\langle z \rangle = \frac{1}{N} \sum_{i=1}^N z_i(t)$ . Then,  $S$  is defined by

$$S = 1 - \frac{1}{M} \sum_{m=1}^M \Theta[\sigma_{\text{th}} - \sigma(m)]. \quad (8)$$

Here,  $\Theta$  is the Heaviside step function and  $\sigma_{\text{th}}$  is a constant threshold value, fixed to 0.1, which is reasonably small. Consequently, the values of  $S = 0$ ,  $S = 1$ , and  $0 < S < 1$  reflect coherent, incoherent, and chimera or traveling wave states, respectively.

The initial conditions for Eqs. (1)–(6) are randomly chosen from a uniform distribution over  $V_i \in (-40 \text{ mV}, 30 \text{ mV})$ ,  $w_i \in (0, 0.4)$  and  $x_j \in (0, 1)$ . Numerical integration of our system is performed using the fourth-order Runge-Kutta algorithm with a fixed time step of  $10 \mu\text{s}$ .

### III. RESULTS

In what follows, we investigate competing dynamical behaviors in chemically coupled nonlocal networks of Morris-Lecar neurons. We begin with a brief review of the bifurcation analysis of the Morris-Lecar model.

#### A. Bifurcation analysis of a type-I Morris-Lecar neuron

Figure 1 shows the bifurcation diagram and the firing frequency response of Morris-Lecar model as a function of applied constant bias current  $I_0$ . In Fig. 1(a), stable (unstable) equilibria corresponding to quiescence states are represented by solid (dashed) lines, whereas stable (unstable) limit cycles corresponding to repetitive firing are shown with filled (empty) circles marking the minimal and maximal membrane voltage amplitudes. Using the parameter set given in Table I, repetitive spiking arises through a saddle-node on invariant circle (SNIC) bifurcation at  $I_0 = 8.33 \mu\text{A}/\text{cm}^2$ . At this bifurcation point, the periodic oscillations, what is referred to as limit cycle, appear with finite amplitude as the saddle and node annihilate. As a result, there exists only an unstable equilibrium surrounded by a stable limit cycle. In this setup, the neuron cannot exhibit bistability. The limit cycles vanish through a saddle-node (SN) bifurcation of the spiking attractor at  $I_0 = 24.18 \mu\text{A}/\text{cm}^2$ , followed by a subcritical Hopf (HB) bifurcation of the equilibrium at  $I_0 = 20.37 \mu\text{A}/\text{cm}^2$  as shown in Fig. 1(a). One can infer the consequences of these bifurcations from Fig. 1(b), which shows the  $(I_0, f)$  curve of the model. It can be clearly noticed that the neuron starts firing with an arbitrary low firing frequency, and the firing frequency rapidly and continuously increases with the increase in the applied bias current over a wide range. As one of the distinctive characteristic properties, this indicates that the neuron is of type-I excitability, which resembles the dynamic behavior of excitatory pyramidal neurons in the cortex [71] that can fire at very low frequency for sustained inputs.

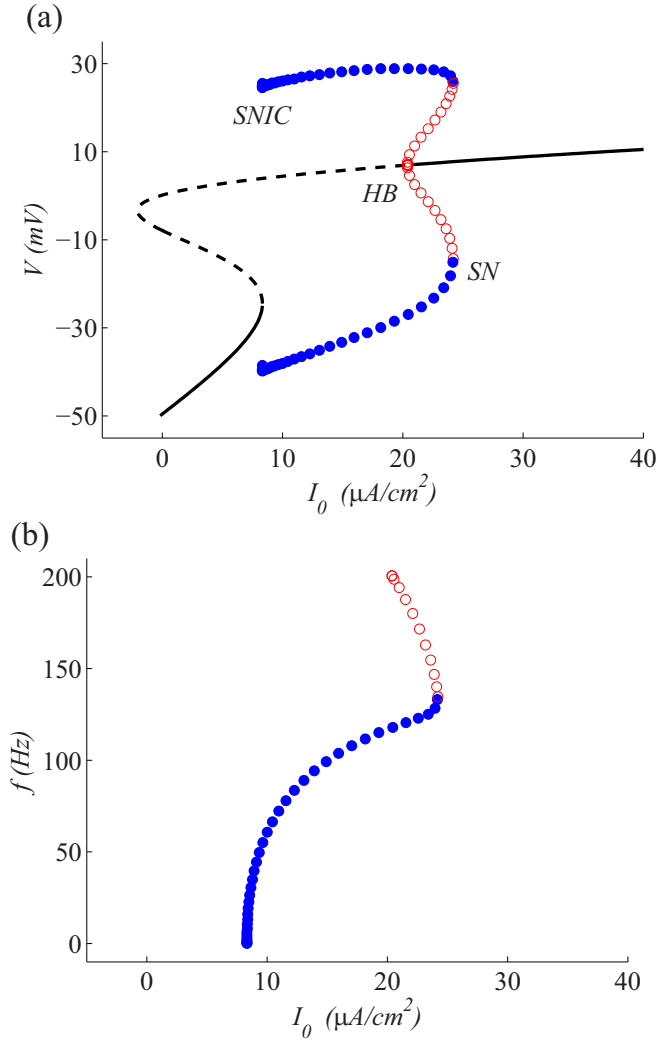


FIG. 1. Panel (a) shows the bifurcation diagram of the Morris-Lecar neuron with type-I excitability as a function of the external bias current  $I_0$ . (thick solid lines: stable equilibria; dotted line: unstable ones; full and empty circles: maxima and minima of stable and unstable limit cycles, respectively). *SNIC*, *HB*, and *SN* mark the saddle-node on invariant circle, Hopf, and saddle-node of limit cycle bifurcations, respectively. Panel (b) represents the corresponding firing frequency vs. current curve ( $I_0$ ,  $f$ ). Evidently, the neuron starts to fire at an arbitrary low firing frequency, which is the distinctive characteristic of type-I excitability. Parameters as in Table I.

### B. Influence of excitability level on population behavior

Next, we investigate the emergence of chimera states with the variation of excitability level accessible by the bias current parameter  $I_0$ . To do so, we consider  $N = 1000$  nonlocally coupled identical Morris-Lecar neurons with fixed coupling radius  $r = 0.1$  and synaptic strength  $g = 0.1$  mS/cm<sup>2</sup>, and picture population behavior by varying  $I_0$ . Obtained results are presented in Fig. 2 where each column illustrates the space-time plots (top panels) and typical snapshots of membrane potentials (middle panels) as well as corresponding average firing frequency profiles (bottom panels) of a given population that is subjected to a fixed  $I_0$ . It is seen that the system under study exhibits characteristically distinct types of

dynamical behaviors as  $I_0$  varies. More precisely, we observe an incoherent state for  $I_0 = 8$  μA/cm<sup>2</sup> at which all the neurons fire asynchronously with the same firing frequency [see Fig. 2(a)]. Population starts to exhibit traveling wave patterns as shown in Fig. 2(b) with a slight increase in  $I_0$  which is set to 10 μA/cm<sup>2</sup>. Then, a further increase in bias current to 11 μA/cm<sup>2</sup>, we observe the chimera state in which the population splits into two domains: coherent and incoherent subpopulations. Top and middle panels illustrating different projections of the population activity in Fig. 2(c) confirm the coexistence of synchronization and desynchronization states within the same population. An arc-shaped average firing frequency profile shown in bottom panel is also another indicator for the emergence of chimera state in a population of type-I Morris-Lecar neurons. To check the persistence of such special behavior, we further increased  $I_0$  and observed that the chimera state does no longer exist, instead a coherent state [Fig. 2(d)] and a global amplitude death [Fig. 2(e)] emerge for  $I_0 = 15$  μA/cm<sup>2</sup> and  $I_0 = 22$  μA/cm<sup>2</sup>, respectively. It can be seen that the population exhibits fully synchronized firings with increased rates in the case of coherent state whereas the coupled neural system is void of oscillations and exhibits a single stable steady state at the emergence of a global amplitude death.

To clearly distinguish these different types of population behaviors and characterize the effect of excitability on their arisals, we compute the  $S$  measure as a function of  $I_0$  for fixed network parameters. The obtained results are presented in Fig. 3. As seen in the figure, a sweep from subthreshold values of  $I_0$  to suprathreshold levels induces five different dynamic behaviors marked by different colors. Note that their respective dynamics were previously illustrated in Fig. 2. Based on extensive simulations, we determine a transition line between traveling waves and chimera states at  $S \approx 0.5$ , which splits the parameter region between incoherence state at  $S = 1$  and coherence state at  $S = 0$  into two distinct divisions. If the applied bias current is chosen in the range of  $8$  μA/cm<sup>2</sup> <  $I_0$  <  $9.25$  μA/cm<sup>2</sup>, we observe that it gives rise to incoherent neural activity, even though it includes insufficient forcing. After the first dynamic behavior threshold, we see traveling waves in the range of  $9.25$  μA/cm<sup>2</sup> <  $I_0$  <  $10.5$  μA/cm<sup>2</sup>. Subsequently, the neural population exhibits chimera states in the applied bias current range of  $10.5$  μA/cm<sup>2</sup> <  $I_0$  <  $12.75$  μA/cm<sup>2</sup>. Eventually, beyond this point, system operates in a coherent state, because the system units are exposed to a sufficiently high bias current. Through the higher excitability levels attained by  $I_0 > 20$  μA/cm<sup>2</sup>, the system exhibits global amplitude death state due to hypersynchronization in the network. Our findings indicate that a population of type-I Morris-Lecar neurons may exhibit different types of synchrony states, including a peculiar chimera behavior, and there are transition regions between them depending on excitability level of individual neurons.

### C. Influence of nonlocal network features on population behavior

We have so far focused on changes in the excitability level to study the emergence of chimera states with fixed network features. In the following, we investigate population dynamics

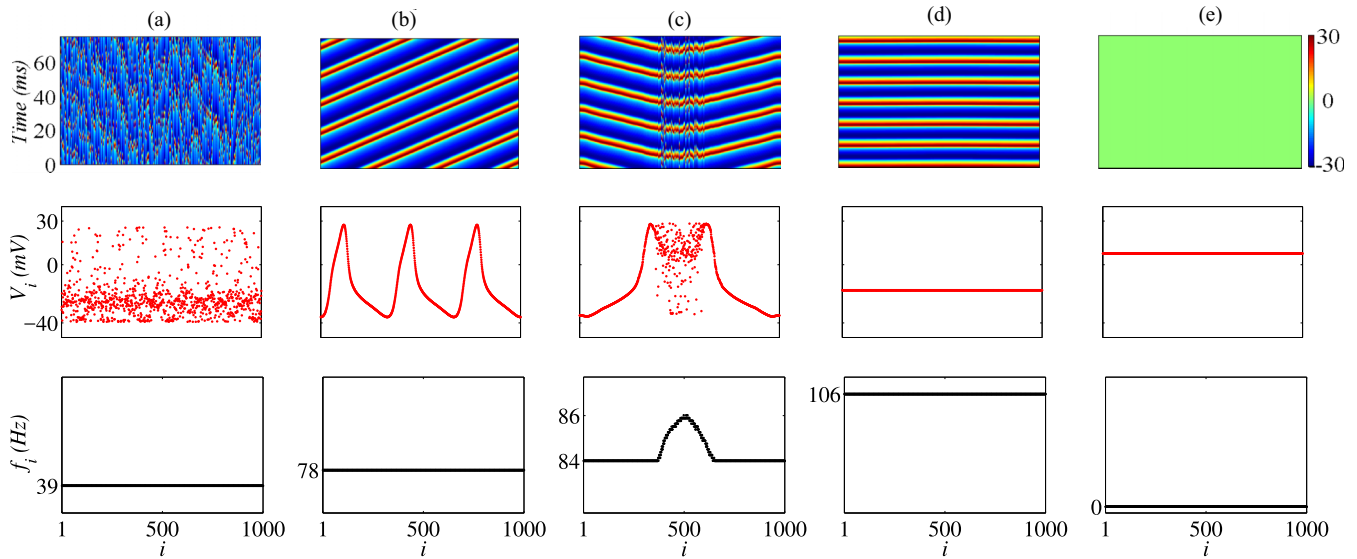


FIG. 2. Influence of the excitability level  $I_0$  on the emergence of chimera states: Increasing the level of excitability gives rise to different system behaviors in nonlocally coupled identical neuron population, i.e., (a) incoherent state, (b) traveling wave, (c) chimera state, (d) coherent state, and (e) global amplitude death for  $I_0 = 8 \mu\text{A}/\text{cm}^2$ ,  $I_0 = 10 \mu\text{A}/\text{cm}^2$ ,  $I_0 = 11 \mu\text{A}/\text{cm}^2$ ,  $I_0 = 15 \mu\text{A}/\text{cm}^2$ , and  $I_0 = 22 \mu\text{A}/\text{cm}^2$ , respectively. Other system parameters are set as  $r = 0.1$  and  $g = 0.1 \text{ mS}/\text{cm}^2$ . Note that each column pictures the space-time plots (top panels) and typical snapshots of membrane potentials (middle panels) as well as corresponding average firing frequency profiles (bottom panels) for a given population that is subjected to a fixed  $I_0$ .

as functions of network coupling radius and synaptic coupling strength. As an extension of the findings about the effect of excitability level on the emergence of chimera states, we now consider four different synchrony states that are shown in Fig. 3 and first seek to determine the influence of network coupling radius in type-I Morris-Lecar neuron populations which operate in, namely, incoherent, traveling wave, chimera, and coherent states. For each case, we analyze the transitions of those behavioral states by varying the coupling radius  $r$  for a fixed value of synaptic strength  $g = 0.1 \text{ mS}/\text{cm}^2$ . Obtained results are given in Fig. 4 that shows variation of  $S$  as a function of  $r$  for different values of  $I_0$ . It is evident that coupling radius  $r$  is a significant system parameter which plays a

major role in determining the emergence of above mentioned synchrony states. For instance, in Fig. 4(a), variation of  $r$  results in emergence of all synchrony states in the population operating with  $I_0 = 8.5 \mu\text{A}/\text{cm}^2$  that has initially ensured incoherent state for  $r = 0.1$  as illustrated in Fig. 3. It is seen that increasing network coupling radius gives rise incoherent, traveling waves, chimera and coherent states to occur when  $r$  lies in the ranges of  $0 < r < 0.12$ ,  $0.12 < r < 0.28$ ,  $0.28 < r < 0.34$  and  $0.34 < r < 0.5$ , respectively. However, these ranges are highly sensitive to changes in  $I_0$ , where the boundary location of each synchrony state tends to shift lower values of  $r$  as  $I_0$  increases. In addition to this, although the range of  $r$  resulting in chimera state does not change very much, the range of  $r$  becomes narrower for incoherent state and traveling waves and wider for coherent state. This indicates that chimera state is robust to variations in excitability level and coupling radius. It is also important to note that traveling waves vanish at very high excitability levels on  $r$  plane [see Fig. 4(d)].

To present a broader perspective on chimera state and to confirm its robustness, we scan a wider interval for  $I_0$  and show population behavior on  $(I_0, r)$  plane as depicted in Fig. 5. It is clear that smaller values of coupling radius support rich population behavior emerging as five different dynamical states whereas larger values only favor coherent state and global amplitude death. Similarly, this is also valid for  $I_0$ , implying that the population exhibits these two later states with increased levels of excitability. Our results reveal that type-I Morris-Lecar neurons are keen on to become synchronized with increased excitability, and however rich population behavior can be observed with relatively low excitability levels and sparse network configuration. The necessity of relative network sparseness for the behavioral variety is due to the role of neighbor numbers in determining total synaptic current introduced into each neuron in the network. More precisely,

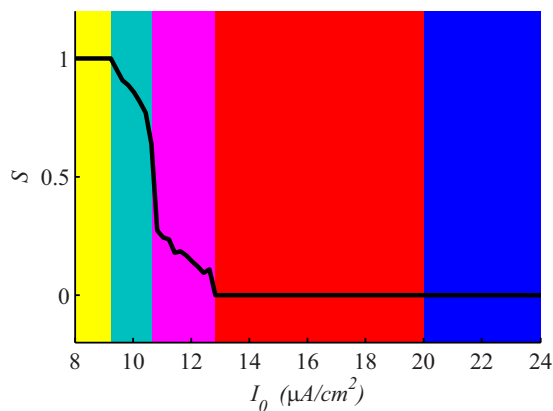


FIG. 3. Strength of incoherence  $S$  as a function of the excitability level  $I_0$ . The color shading indicates five different levels of synchrony: incoherence (yellow), traveling wave (green), chimera (magenta), coherence (red), global amplitude death (blue). System parameters are as described in the caption of Fig. 2.

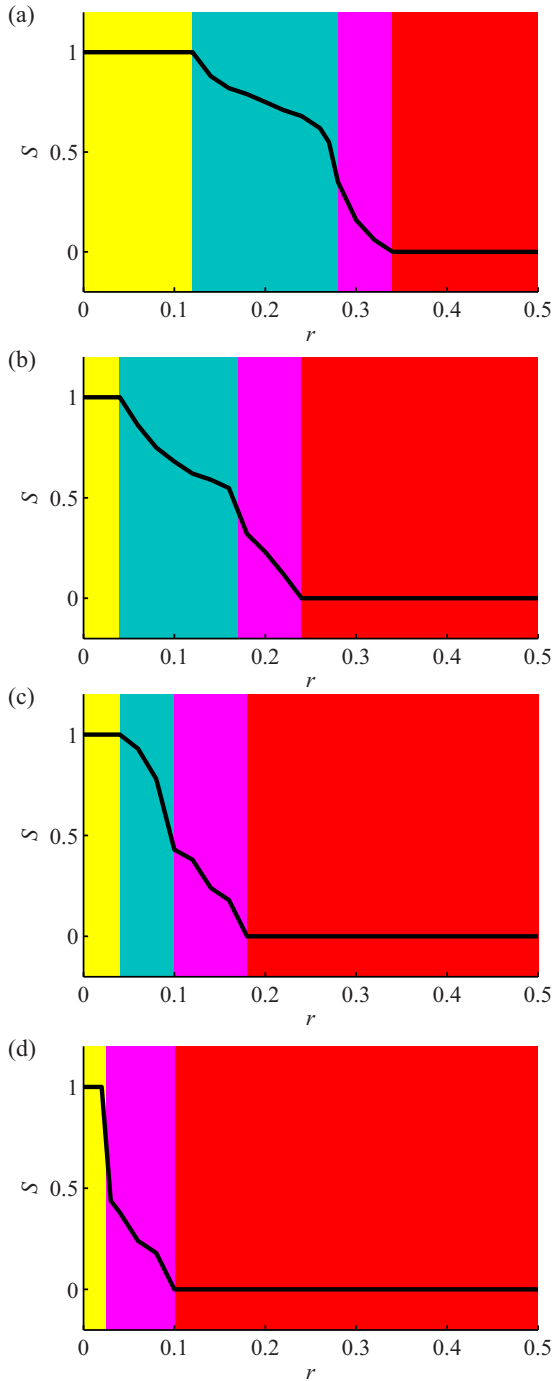


FIG. 4. Effect of coupling radius  $r$  on the emergence of chimera states. Figure shows dynamical behavior transitions with strength of incoherence ( $S$ ) as a function of  $r$  for a fixed coupling strength  $g = 0.1 \text{ mS/cm}^2$  and different excitability levels which are set as: (a)  $I_0 = 8.5 \mu\text{A/cm}^2$ ; (b)  $I_0 = 10 \mu\text{A/cm}^2$ ; (c)  $I_0 = 11 \mu\text{A/cm}^2$ ; (d)  $I_0 = 13 \mu\text{A/cm}^2$ . The color shading indicates different dynamical regimes: incoherence (yellow), traveling wave (green), chimera (magenta), coherence (red).

neurons in a densely connected and homogeneous network topology receive almost identical and very large synaptic inputs which remove the significance of their initial condition inhomogeneity and force them to act simultaneously. More-

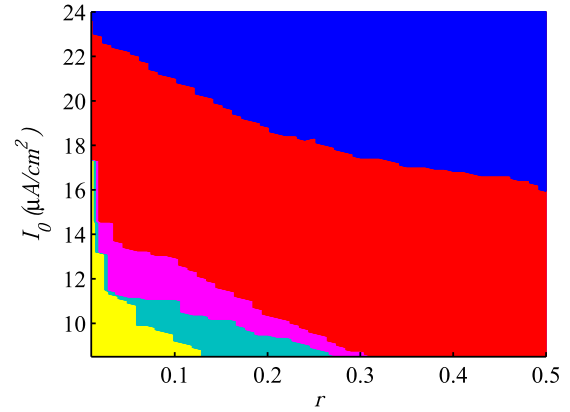


FIG. 5. Effect of excitability level  $I_0$  and coupling radius  $r$  on the emergence of chimera states: incoherent state (yellow), traveling wave (green), chimera state (magenta), coherent state (red), and global amplitude death (blue). The coupling strength is fixed at  $g = 0.1 \text{ mS/cm}^2$ .

over, since the synaptic currents become so large at relatively large values of  $I_0$  and  $r$ , global amplitude death appears in the whole population.

Next, we investigate the behavioral transitions with the joint variation of coupling radius  $r$  and coupling strength  $g$  in our system at a fixed excitability level  $I_0 = 10 \mu\text{A/cm}^2$ . To gain an overall view for coupling parameters' impacts on population dynamics, a behavioral transition map ( $r, g$ ) plane is obtained as shown in Fig. 6. It is obvious that the coupling strength  $g$  has a similar role as coupling radius  $r$ . For instance, consider the effect of  $g$  along on the line of fixed  $r = 0.1$  (see the dashed line in Fig. 6). There exists an incoherent population activity for weak synaptic connections. In this case, the coupling strength is so faint that almost all neurons act as isolated units oscillating independently from their neighbors due to superficial network interaction and very low synaptic current regimes for  $g \in (0 \text{ mS/cm}^2, 0.05 \text{ mS/cm}^2)$ . If the coupling strength is sufficiently increased, the nonlocal

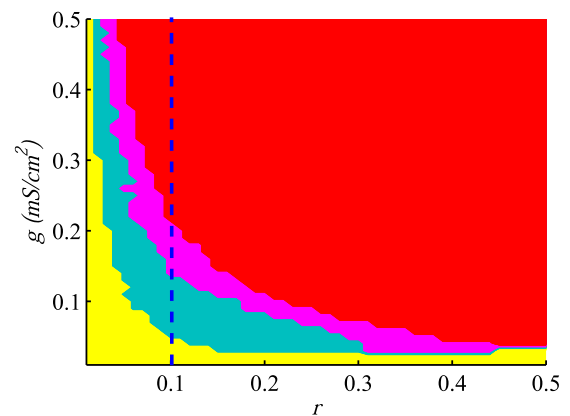


FIG. 6. Behavioral map on ( $r, g$ ) plane for a population which has a fixed excitability level at  $I_0 = 10 \mu\text{A/cm}^2$ . Yellow, green, magenta and red color coded regions represent incoherent state, traveling wave, chimera state and coherent state, respectively. The vertical dashed line marked at  $r = 0.1$  is used as a reference for explanation (see text).

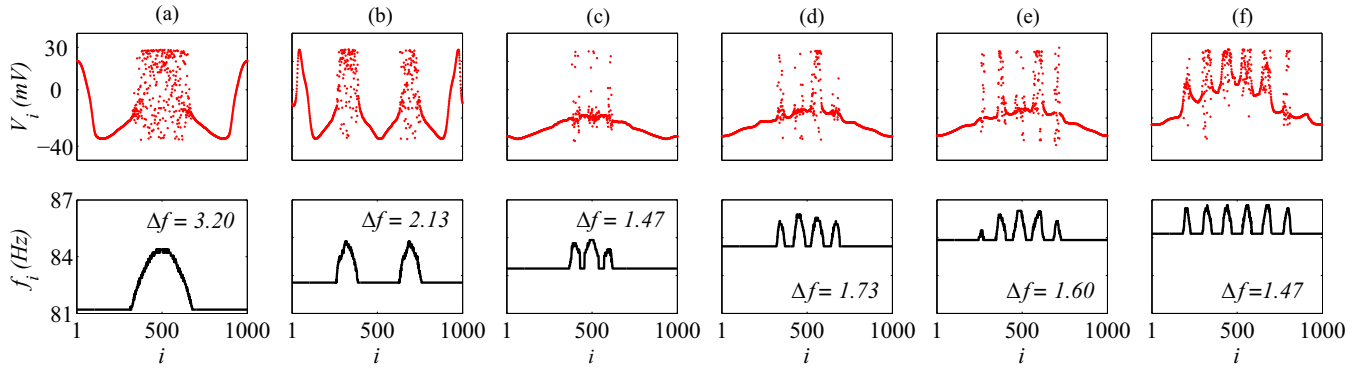


FIG. 7. Emergence of multichimera states with the variation of  $r$  and  $g$ . Top panels show the snapshots of the chimeric population activity splitting into distinct incoherent domains featuring chimera heads. Bottom panels represent average frequency profiles of multichimeras with different numbers of chimera heads. System parameters are fixed as  $I_0 = 10 \mu\text{A}/\text{cm}^2$ ,  $r = 0.1$  in columns (a–c) and  $g = 0.15 \text{ mS}/\text{cm}^2$  in columns (d–f). Coupling strength is set as (a)  $g = 0.16 \text{ mS}/\text{cm}^2$ , (b)  $g = 0.185 \text{ mS}/\text{cm}^2$ , and (c)  $g = 0.19 \text{ mS}/\text{cm}^2$ , while the coupling radius is chosen as (d)  $r = 0.133$ , (e)  $r = 0.138$ , and (f)  $r = 0.143$ .

interaction intensity becomes strong enough to produce extraordinary dynamic behaviors emerging with traveling waves for  $g \in (0.05 \text{ mS}/\text{cm}^2, 0.2 \text{ mS}/\text{cm}^2)$  and chimera state  $g \in (0.2 \text{ mS}/\text{cm}^2, 0.34 \text{ mS}/\text{cm}^2)$ . With a further increase in coupling strength, the complete synchronization emerges and persists in population behavior for  $g \in (0.34 \text{ mS}/\text{cm}^2, 0.5 \text{ mS}/\text{cm}^2)$ . In addition, same behavioral transitions occur if one considers the variation of  $r$  for a fixed  $g$  in the sense that it induces emergence of dynamical behaviors in relatively the same proportion and order. However, it should be also noted that such common effects of these two parameters are valid when neither of them are very small. Now, if we are to evaluate the interaction intensity arising from the combination of two parameters in line with its growth, it is apparent that the system first exhibits incoherent population activity when the nonlocal interaction intensity is too low. This corresponds to a network structure with a few nearest neighbors whatever the value of coupling strength or a weak coupling regardless of number of neighbors. Then, dynamical behavior of the population emerges as traveling waves when the interaction intensity is increased a little more by means of the coupling radius  $r$  and the coupling strength  $g$ . After that, the emergent system behavior occurs as chimera states subsequent to traveling waves, similarly due to increasing the network interaction intensity a little further more. Finally, the system shows coherent population activity, if the network interaction becomes too intense, depending on a strong coupling with a modest number of nearest neighbors or an average interaction strength with a large number of neighbors in a monotonic trend towards higher values of both parameters.

Up to now, we have extensively explored the system parameter regions for which the chimera state exists in type-I Morris-Lecar neuron population. Our aim is now to examine minutely the chimeric behavior of the population by a deep scan of the previously defined chimera regions as functions of network features, i.e.,  $r$  and  $g$ . For this purpose, we first give different representative population activity patterns for randomly selected parameter sets from  $(r, g)$  plane that give rise to emergence of chimera states in Fig. 6. Snapshots of the population activity and corresponding average firing

frequency profiles for different sets of network parameters are shown in Fig. 7. It is seen that there exists extraordinary chimeric states other than the classical one with a single head. In these examples, one can observe that a gradual increase of interaction intensity via both the coupling radius  $r$  and the coupling strength  $g$  results in a reduction of incoherent group size and afterwards emergence of another incoherent subpopulation (top panels). This is also obvious in average frequency profiles of each case where several additional heads emerge indicating that our system of type-I Morris-Lecar neurons exhibits multichimera states (see bottom panels). Further points to be emphasized in these cases are that increasing values of  $r$  and  $g$  induce an increase in average firing frequency of the population (see the base levels of firing frequencies of the coherent parts) and also a reduction in maximal difference between firing frequencies of coherent and incoherent domains ( $\Delta f$ ). Notice that maximal differences for each case are given in bottom panels. The latter finding indicates that all neurons in the population tend to approach each other in phase domain, suggesting that the system will switch to coherent state with further increase of  $r$  and  $g$ .

If we are to bring out explicitly the particular reason behind the occurrence of chimera and multichimera states in type-I Morris-Lecar neurons, our key insight must be that the system under consideration is nonlocally coupled neural population whose dynamic behavior is determined by excitability level of individual cells and essential ingredients of network, i.e., coupling range and coupling strength. Examining the behavior of an isolated neuron and analyzing the network activities, we found that these principal parameters have a relation with the attraction basins of population even though they have diminutive values. As an example of coupling terms' effect, in the case of Parkinson's disease, illness or death of dopamine cells induces a disturbance of balance between synchrony and asynchrony in the basal ganglia, which results in excessive synchronization to arise due to strong coupling between neurons that actually need to be inhibited [24,72,73]. In fact, this balance can be maintained and restored via integrating coupling terms that leads to an increase in the number of stable attractors in the network [74–76], and this gives rise to the emergence of chimera and multichimera states by the cause

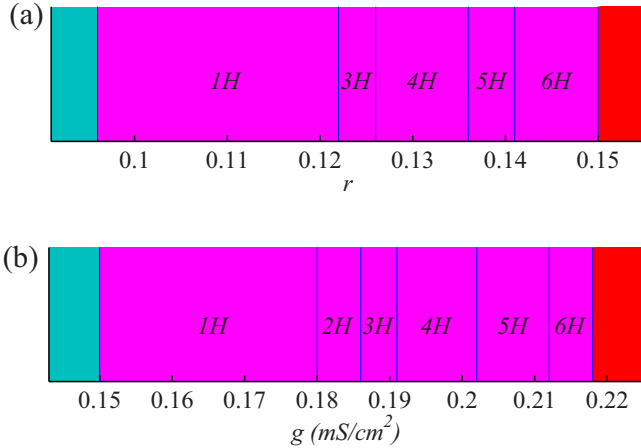


FIG. 8. Effect of  $r$  and  $g$  on the emergence of multichimera states. The figure illustrates multiheaded chimeric behavior of type-I Morris-Lecar neuron population emerging with increasing intensity of network interaction. A single label, for instance  $6H$ , refers to 6-headed chimera states. The excitability level is fixed at  $I_0 = 10 \mu\text{A}/\text{cm}^2$ ,  $g = 0.15 \text{ mS}/\text{cm}^2$  in panel (a) and  $r = 0.1$  in panel (b).

of random initial conditions and increasing coupling strength [68,77]. As a supporting statement, it is recently confirmed that some rare chaotic behaviors require specific choice of coupling terms [78]. In line with this reasoning, we deduce that increasing intensity of network interaction are responsible for the occurrence of multiheaded chimeric behaviors.

To provide a quantitatively distinguishable view, we illustrate the regions of these different chimeras observed with various number of heads in individual parameter scales of  $r$  and  $g$ . Figure 8 shows that there exists certain ranges of  $r$  ( $g$ ) for a fixed value of  $g$  ( $r$ ) giving rise to different multichimeras characterized by number of heads. In Fig. 8(a), one can see that the density of the nonlocal network may give rise to multichimeras up to 6 chimera heads as the coupling radius  $r$  increases, but note that we do not observe a 2-headed chimera state with this parameter scan. In a similar fashion, it is possible to see all multichimera states including a 2-headed chimera with increasing the coupling strength  $g$  [Fig. 8(b)]. Consequently, an intense nonlocal network interaction brings the neural population closer to coherent state (red regions in both figures) since all units begin to oscillate faster and dynamic variables of the system approach to each other. It is important to note here that the nature of fine-structured multichimeras we observed is different from those reported in previous works on nonlocally coupled oscillators of type-I excitability [59]. They rather resemble chimera states reported in lattice limit cycle models [79] and networks of FitzHugh-Nagumo models with a fractal structure [51]. Moreover, the proximity of parameters  $r$  and  $g$  in determining interaction intensity leads us to conclude that attracting basins may be adjusted with the preferable choice.

#### IV. DISCUSSION

In this work, we have verified the occurrence of chimera and multichimera states in a realistic neuron model of Morris-Lecar with type-I neural excitability. Exploring in which

parameter range chimera states can be observed, we have based our investigation of chimera states on excitability level of individual cells and basic ingredients of nonlocal neural network topology, i.e., the coupling radius and the coupling strength. To characterize the observed levels of spatial synchrony, regularity in neuron ensembles has been monitored by the measurements of average firing frequency and the strength of incoherence. Furthermore, since identification of result areas where chimera states and other synchrony types occur is of major importance, the parameter spaces of interest have been systematically scanned. It is found that dynamical population behaviors described above can be reached by changing not only the excitability level  $I_0$  but also coupling strength  $g$  and coupling radius  $r$ . An extensive parameter scan on  $(r, I_0)$  plane has demonstrated that a rich composition of possible dynamic behaviors can be obtained by only low excitability levels and sparse network configuration. Moreover, behavioral map on  $(r, g)$  plane has shown that coupling strength and coupling radius have a close similarity for the occurrence of any dynamic system state. Finally, different chimera and multichimera state patterns have demonstrated the effect of nonlocal network features. To achieve this, changes in chimera behavior have been tracked in the networked system close to the border of synchronization as the interaction intensity grows. We have detected that apart from increase in firing frequency and reduction in maximal difference, stable chimera states first happen to be forked chimera heads, and then continue to split into even finer substructures.

To date, there has been general agreement that ensembles of neural oscillators exhibit great diversity in characteristic dynamic behaviors. Many chimera studies that consider different types of oscillators have also showed that miscellaneous dynamic behaviors appear with different levels of order under variations in parameters of interest. For instance, all behavioral parameter maps presented in Refs. [50,58,80–82] imply that resulting behaviors of each system are diverse under same parameter variations although all dynamical units exhibit type-II excitability of different notation. As for different models of type-I excitability, it is surely predictable that they can also give rise to different behavioral picture on the concerning parameter map. For example, in Ref. [59], coexistence of different multichimera states has been present in a population of type-I saddle-node infinite period oscillators. However, the population of type-I Morris-Lecar neurons here does not exhibit such a coexistence. Moreover, there are incoherent states between different multichimera regions in Ref. [59]. But, our results do not include such an intermittent state. In regards with the appearance of self-oscillations, we find that a moderate interaction intensity is a necessity to observe chimera states in type-I neurons just after the SNIC bifurcation point due to very low firing frequency of individual units. However the case may not be the same in populations of type-II neurons just after the Hopf bifurcation (cf. Refs. [81–84]).

Finally, an important limitation needs to be emphasized. Since we focused on chimera states with the same character as in Kuramoto phase oscillators which is identified by stable manifolds of limit cycles, we used spiking neurons ( $I_0 > 8.33 \mu\text{A}/\text{cm}^2$ ) to investigate the emergence of chimera states under the effect of nonlocal interaction intensity. Therefore,

we did not include the results on chimeric behaviors of excitable neurons ( $I_0 < 8.33 \mu\text{A}/\text{cm}^2$ ). This actually unravels a peculiarity of our study, that is, chimeric behavior in type-I Morris-Lecar neuron population can be observed not only in the excitable regime of isolated units but also in the oscillatory regime depending on the nonlocal interaction intensity (associated with  $r$  and  $g$ ). It is also important to note that initial conditions have a great significance for the emergence of chimera states in the excitable regime. Another unanticipated finding is the level of order in the emergent population behaviors of type-I Morris-Lecar neurons. We observe desynchronization, traveling wave, chimera state, synchronization

and amplitude death. In this context, our findings shed new light on chimera states in neural populations and may also be inclusively promising for future research on the behavior of many different physical and biological systems.

#### ACKNOWLEDGMENTS

M.U. acknowledges support from Erasmus+ programme of the European Union. P.H. acknowledges support by Deutsche Forschungsgemeinschaft within the framework of Collaborative Research Center 910 and under Grant No. HO4695/3-1.

- 
- [1] T. Heil, I. Fischer, W. Elsässer, J. Mulet, and C. R. Mirasso, *Phys. Rev. Lett.* **86**, 795 (2001).
- [2] V. Vlasov and A. Pikovsky, *Phys. Rev. E* **88**, 022908 (2013).
- [3] T. M. Nagiev, *Coherent Synchronized Oxidation Reactions by Hydrogen Peroxide* (Elsevier, Amsterdam, 2006).
- [4] R. Salazar, A. P. J. Jansen, and V. N. Kuzovkov, *Phys. Rev. E* **69**, 031604 (2004).
- [5] C. Li, L. Chen, and K. Aihara, *BMC Syst. Biol.* **1**, 6 (2007).
- [6] R. R. Borges, K. C. Iarosz, A. M. Batista, I. L. Caldas, F. S. Borges, and E. L. Lameu, *Rev. Bras. Ensino Fís.* **37**, 2310 (2015).
- [7] P. J. Uhlhaas, C. Haenschel, D. Nikolić, and W. Singer, *Schizophrenia Bull.* **34**, 927 (2008).
- [8] M. Uzuntarla, E. Barreto, and J. J. Torres, *PLoS Comput. Biol.* **13**, e1005646 (2017).
- [9] Z. Fountas and M. Shanahan, *PLoS ONE* **12**, e0189109 (2017).
- [10] P. Khanna and J. M. Carmena, *eLife* **6**, e24573 (2017).
- [11] A.-L. Giraud and D. Poeppel, *Nat. Neurosci.* **15**, 511 (2012).
- [12] A. Kirschner, J. W. Y. Kam, T. C. Handy, and L. M. Ward, *Front. Hum. Neurosci.* **6**, 139 (2012).
- [13] W. H. Lee, E. Bullmore, and S. Frangou, *NeuroImage* **146**, 724 (2017).
- [14] A. Zalesky, A. Fornito, L. Cocchi, L. L. Gollo, and M. Breakspear, *Proc. Natl. Acad. Sci. USA* **111**, 10341 (2014).
- [15] A. Nini, A. Feingold, H. Slovín, and H. Bergman, *J. Neurophysiol.* **74**, 1800 (1995).
- [16] P. J. Magill, J. P. Bolam, and M. D. Bevan, *Neuroscience* **106**, 313 (2001).
- [17] M. M. Steriade and R. W. McCarley, *Brainstem Control of Wakefulness and Sleep* (Springer Science & Business Media, Berlin, 2013).
- [18] E. Heinrichs-Graham, T. W. Wilson, P. M. Santamaria, S. K. Heithoff, D. Torres-Russotto, J. A. Hutter-Saunders, K. A. Estes, J. L. Meza, R. Mosley, and H. E. Gendelman, *Cereb. Cortex* **24**, 2669 (2013).
- [19] S. Ahn, S. E. Zuber, R. M. Worth, T. Witt, and L. L. Rubchinsky, *Clin. Neurophysiol.* **129**, 842 (2018).
- [20] S. Ahn, L. L. Rubchinsky, and C. C. Lapish, *Cereb. Cortex* **24**, 2553 (2013).
- [21] N. C. Rattenborg, C. Amlaner, and S. Lima, *Neurosci. Biobehav. Rev.* **24**, 817 (2000).
- [22] N. C. Rattenborg, B. Voirin, S. M. Cruz, R. Tisdale, G. Dell’Omo, H.-P. Lipp, M. Wikelski, and A. L. Vyssotski, *Nat. Commun.* **7**, 12468 (2016).
- [23] A. Rothkegel and K. Lehnertz, *New J. Phys.* **16**, 055006 (2014).
- [24] R. G. Andrzejak, C. Rummel, F. Mormann, and K. Schindler, *Sci. Rep.* **6**, 23000 (2016).
- [25] C. R. Laing and C. C. Chow, *Neural Comput.* **13**, 1473 (2001).
- [26] H. Sakaguchi, *Phys. Rev. E* **73**, 031907 (2006).
- [27] Y. Kuramoto and D. Battogtokh, *Nonlinear Phenom. Complex Syst.* **5**, 380 (2002).
- [28] D. M. Abrams and S. H. Strogatz, *Phys. Rev. Lett.* **93**, 174102 (2004).
- [29] D. Tanaka and Y. Kuramoto, *Phys. Rev. E* **68**, 026219 (2003).
- [30] Y. Kawamura, *Phys. Rev. E* **75**, 056204 (2007).
- [31] A. E. Motter, *Nat. Phys.* **6**, 164 (2010).
- [32] A. M. Hagerstrom, T. E. Murphy, R. Roy, P. Hövel, I. Omelchenko, and E. Schöll, *Nat. Phys.* **8**, 658 (2012).
- [33] M. R. Tinsley, S. Nkomo, and K. Showalter, *Nat. Phys.* **8**, 662 (2012).
- [34] E. A. Martens, S. Thutupalli, A. Fourrière, and O. Hallatschek, *Proc. Natl. Acad. Sci. USA* **110**, 10563 (2013).
- [35] T. Kapitaniak, P. Kuzma, J. Wojewoda, K. Czolczynski, and Y. Maistrenko, *Sci. Rep.* **4**, 6379 (2014).
- [36] L. Larger, B. Penkovsky, and Y. Maistrenko, *Nat. Commun.* **6**, 7752 (2015).
- [37] L. V. Gambuzza, A. Buscarino, S. Chessa, L. Fortuna, R. Meucci, and M. Frasca, *Phys. Rev. E* **90**, 032905 (2014).
- [38] M. Wickramasinghe and I. Z. Kiss, *PLoS ONE* **8**, e80586 (2013).
- [39] M. Wickramasinghe and I. Z. Kiss, *Phys. Chem. Chem. Phys.* **16**, 18360 (2014).
- [40] L. Schmidt, K. Schönleber, K. Krischer, and V. García-Morales, *Chaos: Interdisc. J. Nonlin. Sci.* **24**, 013102 (2014).
- [41] E. Montbrió, J. Kurths, and B. Blasius, *Phys. Rev. E* **70**, 056125 (2004).
- [42] G. C. Sethia, A. Sen, and F. M. Atay, *Phys. Rev. Lett.* **100**, 144102 (2008).
- [43] C. R. Laing, *Chaos: Interdisc. J. Nonlin. Sci.* **19**, 013113 (2009).
- [44] N. Yao, Z.-G. Huang, Y.-C. Lai, and Z.-G. Zheng, *Sci. Rep.* **3**, 3522 (2013).
- [45] M. J. Panaggio and D. M. Abrams, *Phys. Rev. E* **91**, 022909 (2015).
- [46] N. Lazarides, G. Neofotistos, and G. P. Tsironis, *Phys. Rev. B* **91**, 054303 (2015).
- [47] T. M. Isele, J. Hizanidis, A. Provata, and P. Hövel, *Phys. Rev. E* **93**, 022217 (2016).

- [48] M. Santos, J. Szezech, F. Borges, K. Iarosz, I. Caldas, A. Batista, R. Viana, and J. Kurths, *Chaos, Solitons Fractals* **101**, 86 (2017).
- [49] J. Hizanidis, N. E. Kouvaris, G. Zamora-López, A. Díaz-Guilera, and C. G. Antonopoulos, *Sci. Rep.* **6**, 19845 (2016).
- [50] S. Majhi, M. Perc, and D. Ghosh, *Chaos: Interdisc. J. Nonlin. Sci.* **27**, 073109 (2017).
- [51] I. Omelchenko, A. Provata, J. Hizanidis, E. Schöll, and P. Hövel, *Phys. Rev. E* **91**, 022917 (2015).
- [52] J. Rinzel, *Bull. Math. Biol.* **52**, 3 (1990).
- [53] R.-G. Xie, W.-G. Chu, S.-J. Hu, and C. Luo, *Int. J. Mol. Sci.* **19**, 161 (2018).
- [54] M. Uzuntarla, J. R. Cressman, M. Ozer, and E. Barreto, *Phys. Rev. E* **88**, 042712 (2013).
- [55] M. Uzuntarla, J. J. Torres, P. So, M. Ozer, and E. Barreto, *Phys. Rev. E* **95**, 012404 (2017).
- [56] Z. Zhao and H. Gu, *Sci. Rep.* **7**, 6760 (2017).
- [57] A. Schmidt, T. Kasimatis, J. Hizanidis, A. Provata, and P. Hövel, *Phys. Rev. E* **95**, 032224 (2017).
- [58] B. K. Bera, D. Ghosh, and M. Lakshmanan, *Phys. Rev. E* **93**, 012205 (2016).
- [59] A. Vüllings, J. Hizanidis, I. Omelchenko, and P. Hövel, *New J. Phys.* **16**, 123039 (2014).
- [60] C. Morris and H. Lecar, *Biophys. J.* **35**, 193 (1981).
- [61] J. Rinzel and G. B. Ermentrout, Analysis of neural excitability and oscillations, in *Methods in Neuronal Modeling*, 2nd ed., edited by C. Koch and I. Segev (MIT Press, Cambridge, MA, 1998), pp. 251–291.
- [62] M. Uzuntarla, *Phys. Lett. A* **377**, 2585 (2013).
- [63] M. Shein-Idelson, G. Cohen, E. Ben-Jacob, and Y. Hanein, *PLoS Comput. Biol.* **12**, e1004883 (2016).
- [64] A. I. Gulyás, M. Megias, Z. Emri, and T. F. Freund, *J. Neurosci.* **19**, 10082 (1999).
- [65] R. Gopal, V. K. Chandrasekar, A. Venkatesan, and M. Lakshmanan, *Phys. Rev. E* **89**, 052914 (2014).
- [66] V. A. Maksimenko, V. V. Makarov, B. K. Bera, D. Ghosh, S. K. Dana, M. V. Goremyko, N. S. Frolov, A. A. Koronovskii, and A. E. Hramov, *Phys. Rev. E* **94**, 052205 (2016).
- [67] A. Mishra, C. Hens, M. Bose, P. K. Roy, and S. K. Dana, *Phys. Rev. E* **92**, 062920 (2015).
- [68] V. K. Chandrasekar, R. Gopal, A. Venkatesan, and M. Lakshmanan, *Phys. Rev. E* **90**, 062913 (2014).
- [69] S. Kundu, S. Majhi, B. K. Bera, D. Ghosh, and M. Lakshmanan, *Phys. Rev. E* **97**, 022201 (2018).
- [70] S. Rakshit, B. K. Bera, M. Perc, and D. Ghosh, *Sci. Rep.* **7**, 2412 (2017).
- [71] T. Tateno, A. Harsch, and H. Robinson, *J. Neurophysiol.* **92**, 2283 (2004).
- [72] G. E. Alexander, *Dialogues Clin. Neurosci.* **6**, 259 (2004).
- [73] L. L. Rubchinsky, C. Park, and R. M. Worth, *Nonlin. Dyn.* **68**, 329 (2012).
- [74] A. Ismail and P. Ashwin, *Dyn. Syst.* **30**, 122 (2015).
- [75] Gokul PM and T. Kapitaniak, *Math. Probl. Eng.* **2017**, 5214235 (2017).
- [76] E. Ullner, A. Zaikin, E. I. Volkov, and J. García-Ojalvo, *Phys. Rev. Lett.* **99**, 148103 (2007).
- [77] N. Yao, Z.-G. Huang, C. Grebogi, and Y.-C. Lai, *Sci. Rep.* **5**, 12988 (2015).
- [78] E. H. Hellen and E. Volkov, *Commun. Nonlin. Sci. Numer. Simul.* **62**, 462 (2018).
- [79] J. Hizanidis, E. Panagakou, I. Omelchenko, E. Schöll, P. Hövel, and A. Provata, *Phys. Rev. E* **92**, 012915 (2015).
- [80] N. Semenova, A. Zakharova, V. Anishchenko, and E. Schöll, *Phys. Rev. Lett.* **117**, 014102 (2016).
- [81] R. Gopal, V. Chandrasekar, D. Senthilkumar, A. Venkatesan, and M. Lakshmanan, *Commun. Nonlin. Sci. Numer. Simul.* **59**, 30 (2018).
- [82] I. A. Shepelev, T. E. Vadivasova, A. Bukh, G. Strelkova, and V. Anishchenko, *Phys. Lett. A* **381**, 1398 (2017).
- [83] A. Zakharova, M. Kapeller, and E. Schöll, *Phys. Rev. Lett.* **112**, 154101 (2014).
- [84] B. K. Bera, D. Ghosh, and T. Banerjee, *Phys. Rev. E* **94**, 012215 (2016).